Analyst

ROYAL SOCIETY OF CHEMISTRY

PAPER

View Article Online
View Journal | View Issue

Cite this: *Analyst*, 2021, **146**, 7583

High-sensitivity small-molecule detection of microcystin-LR cyano-toxin using a terahertz-aptamer biosensor†

Ahmed Mohamed,[a] Ryan Walsh,[b] Mohamed Cherif,[a] Hassan A. Hafez,[c] Xavier Ropagnol,[a,d] François Vidal,[a] Jonathan Perreault[b] and Tsuneyuki Ozaki*[a]

We demonstrate the rapid and highly sensitive detection of a small molecule, microcystin-LR (MC-LR) toxin using an aptasensor based on a terahertz (THz) emission technique named the terahertz chemical microscope (TCM). The main component of the TCM is the sensing plate, which consists of a thin silicon layer deposited on a sapphire substrate, with a natural SiO_2 layer formed on the top of the Si layer. The DNA aptamer is linked to the oxidized top surface of the silicon layer by a one-step reaction (click chemistry) between the DBCO-labeled aptamer and an azido group that binds to the surface. Using density functional theory (DFT) calculations, the number of active sites on the surface has been estimated to be 3.8×10^{13} cm^{-2}. Aptamer immobilization and MC-LR binding have been optimized by adjusting the aptamer concentration and the binding buffer composition. When MC-LR binds with the DNA aptamer, it causes a change in the chemical potential at the surface of the sensing plate, which leads to a change in the amplitude of the THz signal. Compared with other bio-sensing methods such as surface plasmon resonance (SPR), TCM is a rapid assay that can be completed in 15 min (10 min incubation and 5 min data acquisition). Moreover, our results show that the aptamer-based TCM can detect MC-LR with an excellent detection limit of 50 ng L^{-1}, which is 20 times more sensitive compared with SPR measurements of MC-LR.

Received 31st August 2021,
Accepted 5th November 2021

DOI: 10.1039/d1an01577j

rsc.li/analyst

Introduction

Small molecules, in biological sciences, refer to organic molecules with relatively low molecular weight, typically less than 1000 Da in size.[1] This category includes a wide variety of molecules that are biologically, pharmacologically, and environmentally relevant, such as amino acids, peptides, antibiotics and toxins.[2] High sensitivity and rapid detection of these molecules are critical for numerous applications, including drug discovery, diagnostics, and environmental analysis.[3] Conventionally, most small molecules are detected by chromatographic methods, which provide high sensitivity and specificity.[4] However, these methods are limited by their complexity, cost, and long duration of the analysis. Immunoassays are an alternative technique used to detect small molecules, which also demonstrates high sensitivity and selectivity. However, it has a relatively long analysis and procedure time of a few hours and lacks label-free detection since enzymes must be conjugated with secondary antibodies.[5] Surface Plasmon resonance (SPR) is the most well-known optical biosensor for detecting small molecules.[1] SPR benefits from direct, real-time, and label-free detection. However, the detection of small molecules by SPR is challenging because the slight change in the refractive index due to analyte binding leads to very low signal-to-noise ratios, thus increasing the measurement time.[6]

In this work, we demonstrate the highly sensitive and rapid detection of a small molecule, Microcystin-LR (MC-LR), in both buffer and complex samples using a Terahertz Chemical Microscope (TCM) biosensor. Microcystins (MCs, with a molecular weight of 995 g mol^{-1}) are a well-known class of cyano-toxins that induce a harmful effect on animals and human health.[7,8] They are cyclic polypeptides that consist of five constant and two variable amino acids.[9] Exposure to MCs through skin contact and ingestion results in liver failure and may lead to death. Further, MCs inhibit protein phosphatase 1A (PP1A)

[a]*Institut National de la Recherche Scientifique – Énergie Matériaux Télécommunications, Varennes, Québec J3X 1S2, Canada. E-mail: Tsuneyuki.Ozaki@inrs.ca*
[b]*INRS Centre Armand-Frappier Santé Biotechnologie, 531 boulevards des Prairies, Laval, Québec, Canada*
[c]*Fakultät für Physik, Universität Bielefeld, Universitätsstr. 25, 33615 Bielefeld, Germany*
[d]*Département de génie électrique, École de technologie supérieure (ÉTS), Montréal, Québec, H3C 1 K3, Canada*

†Electronic supplementary information (ESI) available. See DOI: 10.1039/d1an01577j

and 2A (PP2A), enzymes that are involved in tumor suppression.[10] MC-LR is the most abundant and toxic cyanotoxin and is distinguished from other MCs by leucine (L) and arginine (R) in the variable amino acid positions.[11] In 1998, the World Health Organization (WHO) declared the acceptable concentration of MC-LR in drinking water to be 1 μg L^{-1} with a total daily intake (TDI) of 0.04 μg kg^{-1}.[12] Therefore, based on these exposure limits, highly sensitive detection and monitoring of such small molecules (typically with a molecular weight under 1000 g mol^{-1}) in drinking water are crucial in preventing and minimizing the health risks associated with MC-LR.

Routinely, MCs are analyzed by high-performance liquid chromatography (HPLC), which is the standard and widely used chemical analytical detection technique.[13] However, HPLC analysis is limited by its complexity, cost, and long duration of the analysis. In addition, it has difficulty separating variants of MCs since they are chemically very similar.[14] Biochemical detection methods such as protein phosphatase inhibition assay (PPIA) and enzyme-linked immunosorbent assay (ELISA) have been used for screening MC variants. PPIA benefits from being an inexpensive and sensitive technique for monitoring the toxicity of MCs and other protein phosphatase inhibitors. The main limitation of this assay is that it is not specific for MCs, which leads to false-positive signals.[15] Antibody-based ELISA is a widely and commonly used biochemical method for MC detection. Although it is sensitive and more specific, it has the highest cross-reactivity among all MC congeners.[16] It also has a relatively long analysis and procedure time, few hours, and lacks label-free detection since enzymes must be conjugated with secondary antibodies. Moreover, the development of reliable antibodies for MC-LR is difficult due to the similarity of different MC variants.[17] On the other hand, aptamers, synthetic single-stranded DNA or RNA with certain sequences, have the ability to bind to their targets with high sensitivity and selectivity. The main advantages of using aptamers over presenting enzymes and antibodies are the ease of selection, low cost of the synthesis process, and higher stability under different environmental and detectable conditions. Ng *et al.* succeeded in developing new aptamers that have a high binding affinity (K_D ranging from 28 to 60 nM) and selectivity to MC-LR, -YR, and -LA.[18] In parallel, rapid, simple, robust, and specific biosensors based on different detection techniques based on optical and electrochemical principles have been applied to MC screening. Surface Plasmon resonance (SPR) is the most well-known optical biosensor for detecting MC-LR. SPR benefits from direct, real-time, and label-free detection. However, it has difficulty detecting small molecules and it has quite a lengthy analysis time, typically of approximately 50 min[19]

Terahertz (THz) waves, whose frequencies range from 0.1 to 10 THz, have unique characteristics, such as being transparent to plastic, paper, clothes, ceramic, and being strongly absorbed by some particular molecules such as water, explosives and drugs.[20] Due to its low photon energy (4 meV at 1 THz), these waves are also non-ionizing and results in no or minimal damaging effects to humans, unlike X-ray. Recently, THz technologies are attracting significant interest, profiting primarily from the rapid progress in ultrafast lasers, opening access to a wide range of applications. For example, THz technology is used for sensing and characterizing different materials using the popular THz time-domain spectroscopy technique[21,22] and in various imaging techniques such as a single-pixel detector and compressed sensing.[23] Compared with other spectroscopy methods, THz time-domain spectroscopy (THz-TDS) has many advantages, such as providing distinct molecular spectral fingerprints, and the ability to determine the complex conductivity of material without assuming the Kramers–Kronig relation. However, the sensitivity of techniques using THz radiation is strongly affected by the large THz absorption of water, with an absorption coefficient of 220 cm^{-1} at 1 THz.[24,25]

To overcome this limitation, which is especially important in biological and chemistry applications, a new technique based on THz emission, named the THz chemical microscope (TCM), has been invented by T. Kiwa and his coworkers.[25] TCM is a multifunctional and adaptive THz sensor that can be used to sense and monitor, by raster scanning, the change in the chemical potential occurring at the surface of the sensing plate. The sensing plate is the key component that consists of three layers (sapphire substrate, silicon, and natural SiO_2). Recently, the TCM was successfully used to detect breast cancer cells, with a limit of detection (LOD) of 1 cell per 100 μL, by modifying the sensing plate with aptamers.[26] Although the SPR sensor has many advantages for detecting large molecules, it faces a challenge to detect small molecules such as mannose,[19] since small molecules cause smaller (barely observable in some cases) changes in the refractive index of the sensor material. SPR has been studied to detect MC-LR,[27] demonstrating an LOD of 1–100 μg L^{-1}, a sensitivity insufficient for the early monitoring of MC-LR. Further, the relatively long detection time (50 min) for the SPR detection of MC-LR is another limitation. Therefore, developing and optimizing novel techniques for highly sensitive and rapid detection of small molecules such as MC-LR are urgently needed in environmental monitoring.

Here, we report the development and optimization of a THz-aptamer sensor based on the TCM to detect MC-LR in buffer and complex samples. The TCM aptasensor performance was improved by optimizing several parameters such as the number of active sites on the surface of a sensing plate, the aptamer concentration, the binding buffer composition (Mg^+ ion concentration and pH), and incubation time of the MC-LR sample.

Experimental section

Materials and methodology

MC-LR was purchased from Cedarlane Labs, Burlington, Canada. The stock MC-LR sample was diluted in the binding buffer (50 mM Tris, 1 mM $MgCl_2$, and pH 7.4). A complex water sample collected from the Saint Lawrence River in

Montreal, Canada, was spiked with a specific concentration of MC-LR solution. To optimize binding conditions, the binding buffer was prepared at different pH values (3.4, 7.4 and 8.5) and with different Mg concentrations (0.5, 1 and 2 mM). The MC-LR DNA aptamer was purchased from AlphaDNA, Montreal, Canada. The MC-LR aptamer, AN-6[18] was labeled on the 5′ end through an amine modification which was reacted with dibenzocyclooctyne (DBCO) N-hydroxysuccinimide (NHS) Ester (AAT Bioquest, Sunnyvale, USA) by AlphaDNA (Fig. S1†)

DBCO-ATACCAGCTTATTCAATTGGCGCCAAACAGGACCACC-ATGACAATTACCCATACCACCTCATTATGCCCCATCTCCGCAGAT-AGTAAGTGCAATCT

Different concentrations of the DBCO-aptamer (0.01 to 10 μM) were prepared by diluting the 50 μM stock with milliQ water. 3-(Azidopropyl) triethoxysilane (AzPTES) used for surface silanization was purchased from Gelest, Morrisville, USA. The antibiotics used for negative control experiments, kanamycin sulfate (50 mg ml^{-1}) and ampicillin sodium salt (100 mg ml^{-1}), were respectively purchased from Bio Basic Inc. Markham, ON, Canada; and Sigma, Oakville, ON, Canada. The antibiotics were diluted in the binding buffer (50 mM Tris, 1 mM $MgCl_2$ and pH 7.4) before use.

Surface functionalization is the most critical step in biosensor fabrication since it increases the biosensor sensitivity and reduces nonspecific adsorptions. To bind the aptamer 'receptor' to the SiO_2 surface, the surface was covalently modified (silanized) using organosilanes. Before silanization, the surface was cleaned with ethanol (Sigma-Aldrich) and milliQ water. Then the surface was activated by immersing the sensor plate in 1 M NaOH (Sigma-Aldrich) for 10 min, followed by rewashing with ethanol, PBS buffer, and finally milliQ water. For the silanization process, the plate was immersed in 100 μM of AzPTES aqueous solution for 30 min. This molecule, AzPTES, contains an azido group that interacts with the DCBO group on the DNA in one step click chemistry addition, covalently linking the aptamer to the surface. Following silanization, the surface was extensively washed with ethanol, PBS buffer and milliQ water. Then the sensing plate was dried at 105 °C for 2 hours.

To establish an efficient binding of DCBO-aptamer to the sensing surface, the surface plate was incubated with various aptamer concentrations ranging from 0.01 to 10 μM, along with various incubation times. Finally, the sensing plate was rewashed with ethanol, milliQ water, and the binding buffer. To determine the LOD of the TCM, MC-LR ranging in concentration from 0.1 nM to 1 μM was incubated on the surface of the sensing plate for 10 min. MC-LR solutions were prepared in the binding buffer. The TCM biosensor was tested to study how accurately it can detect MC-LR in a complex water sample by spiking the real-world water sample with 0.1 nM of MC-LR. The TCM chip was regenerated by incubating 50 mM of NaOH on it for 1–2 min. The chip was subsequently washed with binding buffer and milliQ water. Negative control experiments were done by incubating the TCM chip in 1 μM of kanamycin and ampicillin antibiotics prepared in the binding buffer.

Physical principle and optical setup

The key component in the TCM system is the sensing plate, as depicted in Fig. 1. It consists of a silicon (Si) thin film deposited on a sapphire substrate (MTI Corporation, CA, USA). The thickness of the Si and sapphire substrates are 600 nm and 500 μm, respectively. A thin layer of natural oxide, 2–3 nm thick, forms on the Si surface. The SiO_2 layer isolates the Si thin film from contact with electrons involved in the chemical interactions. In addition, the oxide is an appropriate substrate for functionalization. In principle, at the interface between Si and SiO_2, the chemical potential (or equivalently Fermi energy) of the surface states, E_{Fs}, is not the same as that of the bulk states E_{Fb}. Therefore, Fermi level pinning causes a 'bending' of the valence and conduction bands at the interface.[28] Electrons are then depleted away from this area, and a depletion electric field is formed. When a beam of femtosecond laser pulses, with photon energy higher than the bandgap (1.12 eV at 300 K) of Si, is focused on the sensing plate from the sapphire substrate side, electrons in the Si layer are excited from the valence band to the conduction band. Then, they are accelerated by the depletion electric field, leading to the generation of a photocurrent.[29] The variation in the photocurrent density generates broadband THz pulses that are emitted from the Si layer and then radiated into free space. Fig. S2† describes schematically the change in the THz amplitude when chemical reactions proceed on the sensing plate. Briefly, chemical reactions induce charges to be redistributed on the surface, which leads to a shift in the chemical or electric potential 'VBB' at a certain depth, Z, in the Si layer, thereby changing the magnitude of the depletion electric field. At a certain depth, Z, in the Si bulk, the depletion electric field ($E_l(Z,t)$) is linearly proportional to the square root of the chemical potential and is given by[30]

$$E_l(Z,t) = \sqrt{\frac{eN_{d(t)}}{2\varepsilon}} \times \sqrt{V_{BB}(Z,t)} \quad (1)$$

where N_d is the carrier density, which is dependent on time, e is the electron charge, and ε is the dielectric constant of the Si layer. According to Maxwell's equation, the radiated electric field is proportional to the time derivative of the current density:

$$E_{THz}(t) \propto \frac{\partial J}{\partial t} \quad (2)$$

with the current density is:

$$J(t) = e\mu N_d(t) E_l(Z,t) \quad (3)$$

combining eqn (2) and (3), we obtain:

$$E_{THz}(t) \propto e\mu \left(E_l(z,t) \frac{\partial N_d}{\partial t} + N_d(t) \frac{\partial E_l(Z,t)}{\partial t} \right). \quad (4)$$

Here, eqn (4) describes the temporal dependence of the THz electric field. In the TCM, the full temporal waveform of the THz pulse is not important, since we only monitor the maximum amplitude of the THz pulse. Consequently, in the

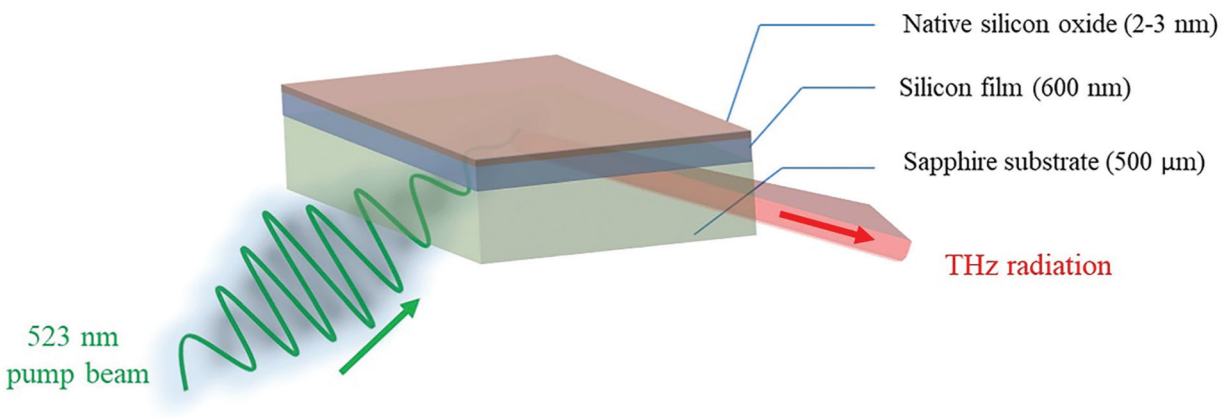

Fig. 1 Schematic diagram showing the composition of the sensing plate and the excitation – detection configuration.

case where the chemical reaction and the variation of the chemical potential are extremely slow *versus* the variation of the carrier density, we can estimate the depletion field to be independent of time on the timescale of the duration of the THz pulse and (4) can be rewritten as:

$$E_{\mathrm{THz}}(t) \propto E_{\mathrm{l}}(z) e\mu \frac{\partial N_{\mathrm{d}}}{\partial t}. \quad (5)$$

From eqn (5), we can see that the THz field is linearly proportional to the depletion field.

Fig. S3† depicts the optical setup of the TCM system. Femtosecond laser pulses are generated from an ytterbium (Yb)-doped oscillator laser (HighQ-2, Newport Spectra-Physics, CA, USA). The Yb laser has a central wavelength of 1045 nm, an average power of 700 mW, a repetition rate of 63 MHz, a bandwidth of 6 nm, and a pulse duration of 250 fs. The fundamental beam (1045 nm) is split into two beams, pump and probe, with an optical beam-splitter. The pump beam is frequency-doubled using a type I BBO crystal with 2 mm thickness to generate the second harmonic (522 nm). The maximum conversion efficiency of the BBO crystal is around 45%, and the maximum power at 522 nm is approximately 290 mW. The 1045 nm beam is filtered using a colour filter (FGB37-A, Thorlabs, NJ, USA). Since we use lock-in detection with a mechanical optical chopper placed in the pump beam path after the color glass filter, the optical power onto the sensing plate is 145 mW. A metallic mirror placed before the sensing plate sends the beam at an incidence angle of 45°. The generated THz radiation is radiated into free space. However, only the reflected THz pulses are collimated and focused onto the THz detector (bPCA-3000-05-10-1060, Bowtie photoconductive antenna, BATOP, Germany) using a pair of off-axis parabolic mirrors. The power of the probe laser used for the Bowtie detector is 20 mW. The pump beam is mechanically chopped at a frequency of 300 Hz, lock-in detection and a current amplifier are employed to improve the signal-to-noise ratio of the measurements with an integration time of 1.5 seconds. Photoconductive sampling is performed to detect the THz electric field profile by varying the time delay between the pump and probe laser pulses. However, in the specific cases of the TCM, we only probe the time variation of the peak electric field, which is at the same time scale variation of the chemical potential, or we monitor the variation of the THz peak field over the full area of the sensor by raster scanning. For the THz measurements, we fix the delay at the peak of the THz field. The sensing plate is mounted on an *x*–*y* translational stage and raster-scanned with a spatial increment of 0.2 mm per step to acquire a map of the peak THz field in 2D as depicted in Fig. S4.†

The TCM direct assay is performed by injecting the binding buffer or MC-LR samples over the aptamer-functionalized TCM chip (side of SiO_2 layer). The optical pump beam hits the Si/SiO_2 interface from the backside (sapphire side), and the THz emission is detected in the specular reflection direction, as shown in Fig. 1. This configuration results in the THz beam not passing through the aptamer-sample solution. Therefore, the TCM biosensor has a significant advantage over the conventional THz-TDS method, since for the former, the THz radiation would not be absorbed by water solution. The first step in the TCM assay is performed by scanning the THz peak maximum emitted from the most uniform part in the functionalized plate (2 mm × 2 mm) with/without immobilized aptamers. Then, the TCM baseline has been obtained by adding the non-spiked samples (buffer or complex) to the sensing plate's surface. Afterwards, the aptamer-MC-LR binding was measured by incubating the spiked samples (buffer or complex) with different concentrations (0.1 to 1000 nM) for 10 min on the chip surface. The MC-LR analyte must be removed to reuse the sensor chip, but the aptamer must stay intact. Therefore, the regeneration process should be performed by adding a denaturation solution (50 mM NaOH) on the surface for 1–2 min. In principle, the alkaline medium increases negative charges, which temporarily destabilizes bonds between guanine and thymine, thus breaking out the

hydrogen bonds between the two DNA helixes. In this way, the NaOH solution with the unbound MC-LR molecules is swept away. Then the binding buffer is directly added to the chip surface to reform the aptamer structure. Eventually, the TCM signal returned to the baseline level, and thus the sensor chip is ready to be reused.

Density functional theory (DFT) calculation

DFT calculations were performed to provide theoretical insight into the surface density of the AzPTES, used for silanization of the SiO_2 layer, which is equivalent to the surface density of aptamer molecules. All the DFT calculations reported here were done using the Vienna *ab initio* software package (VASP).[31–34] The calculations were performed without magnetic effects using the generalized gradient approximation (GGA) with the Perdew–Burke–Ernzerhof (PBE) functional.[35] The convergence criterion on the relative energy was set to 10^{-5}, and the plane wave energy cut-off was set to 520 eV for all calculations. The Brillouin zone was sampled on regular $1 \times 1 \times 1$ gamma grids. An α-quartz SiO_2 structure with cell dimensions of a = 5.02 Å and b = 7.25 Å and c = 8.70 Å was used as a model for the SiO_2 surface. A void of 33 Å was included in the normal direction to avoid interactions between the periodic SiO_2 layers. The active and inactive molecules were adsorbed on the free surface of SiO_2. The positions of all the atoms were fully relaxed, and the binding energy of an AzPTES molecule (the adsorption process is explained in the ESI†) on a given site was calculated using

$$E_b = (E_{SiO_2 * AzPTES} + E_{H_2O}) - E_{SiO_2} + E_{AzPTES} \quad (6)$$

where $E_{SiO_2+AzPTES}$ is the energy of the SiO_2 layer with AzPTES, E_{SiO_2-H} is the energy of the SiO_2 layer alone covered with hydrogen on the surface, E_{AzPTES} is the energy of AzPTES far from the SiO_2 layer, and $E_{H_2O}$is the energy of the formed water.

Each step of the sequence (3) corresponds to a free energy given by

$$G = G_0 + ZPE + Tds + G_{sol} \quad (7)$$

where G_0 is the energy of the structure per cell, ZPE is the zero-point energy, Tds is the entropy term, and G_{sol} is the solvation energy arising by the aqueous medium. As followed in some previous works,[36–38] for simplicity, we will assume that the sum of the last three contributions nearly cancels, in apparent agreement with past works.[39,40]

Results & discussion

Surface functionalization

In this work, we investigate the capability of the TCM biosensor platform to efficiently detect MC-LR toxin by using the specific and selective DNA aptamer with a dissociation constant (K_D) of 50 nM. The binding of MC-LR to the immobilized aptamer resulted in a change in chemical potential at the sensing plate surface and consequently, a change in the THz amplitude. Optimization of the conjugation time, in this case, the time needed for the aptamer's DBCO chemical group to react with the azido group from the AzPTES on the sensor surface (Fig. S1†), and the concentration of MC-LR aptamers are important, like in any biosensor, for maximizing the sensitivity of the TCM. In Fig. 2A, one can see that the THz amplitude quickly increased and stabilized after one minute (1 min) of conjugation with the aptamer by click-chemistry. No further change in the THz signal amplitude was observed with conjugation time longer than 1 min. This result shows that the aptamer is quickly conjugated to the sensing plate surface. Fig. 2B shows the change in the THz amplitude by varying the concentration of the aptamer (between 0.01 to 10 μM). The maximum THz signal amplitude was observed at 1 μM aptamer concentration, and then it decreased when the concentration increased to 10 μM. This reduction, at 10 μM, might be interpreted by electrostatic repulsions between aptamers that result from negatively charged sugar-phosphate

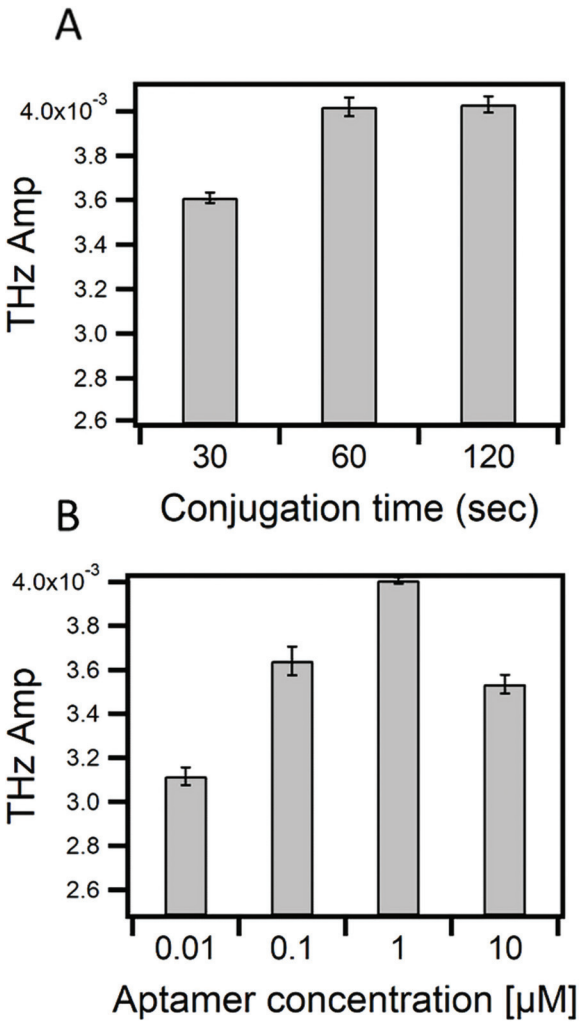

Fig. 2 Aptamer conjugation to the sensor surface [A] THz amplitude as a function of conjugation time of the aptamer and [B] the effect of aptamer concentration on the THz signal amplitude. Values are shown as means ± S.E.M. of three trials.

backbone of DNAs.[41,42] Therefore, we could have maximum coverage of the sensing plate surface at 1 μM of the aptamer that would drastically minimize the probability of nonspecific adsorptions. The number of aptamer molecules dissolved in 65 μL at 1 μM is approximately 3.9×10^{13} cm^{-2}. For uniform immobilization of aptamers on the surface, each aptamer molecule would bind to one AzPTES molecule (active site).

The number of active sites on the sensing surface, which is equivalent to the number of aptamer molecules, was estimated by DFT calculations. The selection criterion for estimating the number of active sites is the binding energy of an AzPTES molecule with the surface (Si-OH) as a function of the AzPTES surface density. The configuration that gives the lowest binding energy corresponds to the most likely density of active sites. To generate different AzPTES surface densities, we created different super cells with repetition of the elementary cell in the *x*–*z* plane and place a single AzPTES molecule on the surface. The different super cells, their areas, and the surface density of AzPTES are shown in Table S1.† Fig. 3 shows the binding energy as a function of the number of the AzPTES surface density. The results show that a high concentration of AzPTES molecules cannot be adsorbed on the surface since the binding energy is close to 0 eV, whereas for the super cell (3 × 1 × 2) (Fig. S8†), which has a surface density of AzPTES molecules of 3.8×10^{13} cm^{-2}, the binding energy is the lowest with −5.17 eV. The adsorption of this molecule takes place in a free area of 262.5 $Å^2$. In this case, the molecule will be able to tear off the hydrogen atom and take place in an exothermic sense of the reaction. We have also noticed that adsorption is possible at lower concentrations but with higher energy values. This result is in perfect agreement with the experimental observation. All the details of the calculations are given in the ESI.†

Highly sensitive detection of MC-LR

The binding of MC-LR to its aptamer might be affected by several factors such as the presence of ions (Mg^{2+}, Na^{+}) in the binding buffer, pH, and incubation time of MC-LR on the surface. Therefore, studying these factors is crucial for having a reliable and sensitive detection of MC-LR toxin. Fig. 4A shows the change in the THz amplitude with an increase in incubation time of the sample on the apta-sensing surface. The THz signal reached its maximum after 10 min, and no further change was observed past that incubation time. Therefore, the TCM assays can be completed in 15 min (10 min incubation and 5 min data acquisition). As compared with other biosensors such as SPR and ELISA,[27] the TCM platform offers a rapid assay for the detection of MC-LR. Fig. 4B describes the effect of the pH on the binding of MC-LR to the aptamer. At pH 7.4, the THz signal was the highest compared with the acidic (pH 3.4) and the basic (pH 8.5) media. This effect might be attributed to a change in the conformation of the DNA at different pHs as the secondary structure of DNA aptamers is heavily dependent on hydrogen bond formation. Additionally, the ligand MC-LR is negatively charged and changes its valence at different pH values ($3 < pH < 13$).[43] Mg^{2+} ion concentration is another parameter that may affect the binding of MC-LR as it will affect the conformation of the aptamer. Fig. 4C shows that 1 mM of Mg^{2+} ions is the optimum concentration for achieving the best binding of MC-LR to the aptamer.

To estimate the limit of detection in these optimized conditions, different concentrations (0.1 nM to 1 μM) of MC-LR were incubated on the surface of the sensor. Fig. 5A shows TCM images that have been obtained by subtracting the baseline (buffer) value. It is observed that the THz change increases with increasing MC-LR concentrations. Fig. 5B represents the linear relationship between the logarithm of the MC-LR concentration and the THz amplitude. Meanwhile, the LOD of the TCM was calculated to be 0.05 nM (50 ng L^{-1}). This value was evaluated from the standard deviation of the signal that is higher than that of the buffer signal, multiplied by three and added to the background (3 × SD).[44] The results show that the LOD of our aptamer-based TCM is 20 times smaller than that of the SPR,[27] making it a superb biosensor for MC-LR with high sensitivity and speed compared with other biosensors.[45,46] SPR has been the standard and widespread biosensor in the last few decades because it provides a real-time, label-free, and sensitive detection method for different biological entities. However, our new TCM biosensor has several advantages compared with it. First, the SPR has low sensitivity for directly detecting small-size molecules (<1000 Da), since it causes only small changes in the refractive index at the SPR interface. Therefore, the SPR signal would be comparable with the noise level (baseline) of the system.[47] This situation has been handled by using indirect (inhibition or competitive) detection methods. Unfortunately, these indirect methods create disadvantages, such as slowing down the analysis time and labelling recognition elements. Second, the detection of large organisms such as large bacteria is limited. Since the sensitivity of the SPR biosensor is based on the electric field decay length of the surface plasmon waves (around 200 nm for the gold SPR chip), which is perpendicular to the

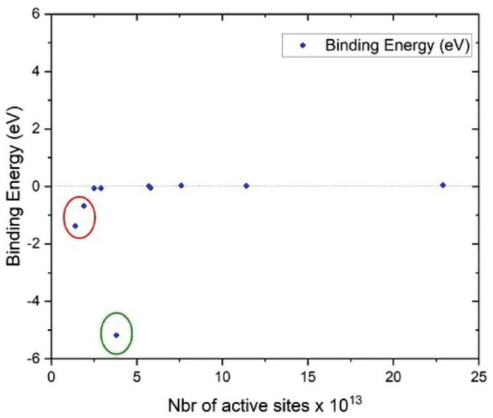

Fig. 3 Calculated binding energy as a function of the AzPTES concentration on the surface (SiO_2). Green circle: optimal concentration, red circle: low concentration.

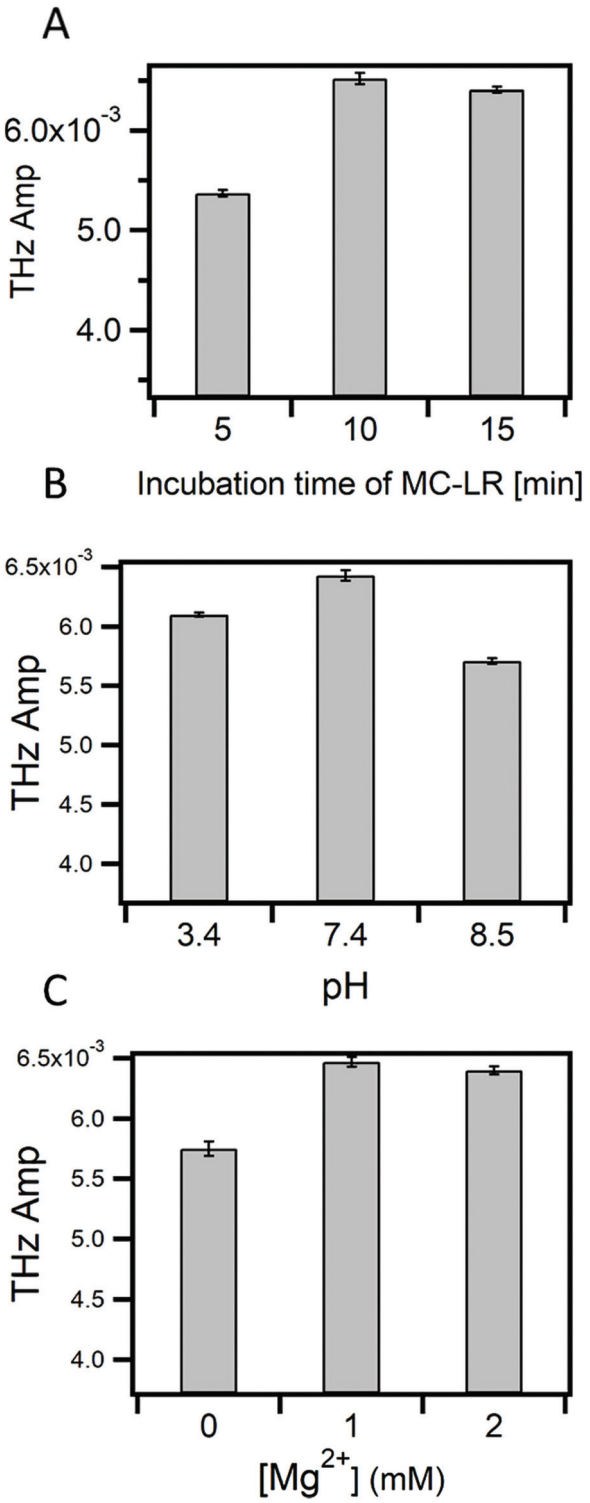

Fig. 4 Optimization of binding conditions. [A] Change in the THz signal amplitude with an incubation time of MC-LR aptamers. [B] Effect of pH of the binding buffer on the TCM response. [C] Effect of Mg^{2+} concentration on the THz response of the TCM system. All these experiments were done with 100 μM of MC-LR. Values are shown as means ± S.E.M. of three trials.

surface. The larger the decay length, the higher the sensitivity of large organisms. Increasing the penetration decay length to cover the entire volume of the large entity (*e.g.* bacteria) would, in turn, increase the perturbation of the SP electric field that is very sensitive to changes in the optical properties of the dielectric solution adjacent to the metal surface.[48] Third, the SPR configuration is complicated as a prism coupler must be set to efficiently couple the light and the surface plasmon momentums by increasing the light's momentum and achieving the total internal reflection (TIR) condition. On the other hand, our TCM biosensor is easy to use and more sensitive for detecting small and large biological entities. This characteristic results from the detection concept of the TCM biosensor in which the charge redistribution takes place between molecules in the first layer directly contacted to the surface regardless of the size of entities. At the end of this part, it would be better to remind that one of the major drawbacks of THz-based biosensing is strong absorbance by water, but this is circumvented by the TCM set-up.

To demonstrate the capability of the TCM biosensor for detecting a low concentration of MC-LR in a complex sample such as river water, the THz signals from the buffer and river samples are compared, whose results are shown in Table 1. The THz change in the case of non-spiked and spiked river water with 0.1 nM of MC-LR is lower than that in the non-spiked and spiked buffer solutions. The recovery of the TCM sensor for the spiked river water is low, around 70%, which indicates a significant difference in the behaviour of the sensor to the complex spiked sample. It might be attributed to the salt content as the river water complex has a low amount compared to the buffer sample. Hence, 0.1 volume of 10× buffer was added to the river sample to adjust the pH and increase the salt concentration to be roughly similar to the buffer salt content, *i.e.* 1 mM. This addition improved the recovery of the TCM aptasensor up to 94%, which refers to the potential role of the salt content for the TCM sensor's performance. The remaining slight difference in the THz signal between the two samples might result from impurities and unwanted compounds that have non-specific interactions with the aptamer/MC-LR system. Accordingly, the LOD is comparable to that of the buffer solution, 50 ng L^{-1}, which is much lower than the maximum acceptable concentration (MAC) of Canadian regulation for drinking water, which is 1.5 μg L^{-1}. Therefore, TCM has a good recovery for detecting the MC-LR toxin in a real-world water sample, which shows that it would be a promising biosensor candidate for monitoring water quality.

The selectivity of biosensors is one of the most important parameters that should be studied. Beyond the fact that the AN-6 MC-LR aptamer can specifically recognize MC-LR and no other microcystins,[18] it is vital to ensure that other types of molecules will not interfere with the biosensor. We performed negative control experiments using kanamycin and ampicillin, which are positively charged and negatively charged antibiotics, respectively. They were individually incubated at a concentration of 1 μM in binding buffer containing 1 mM Mg^{2+}

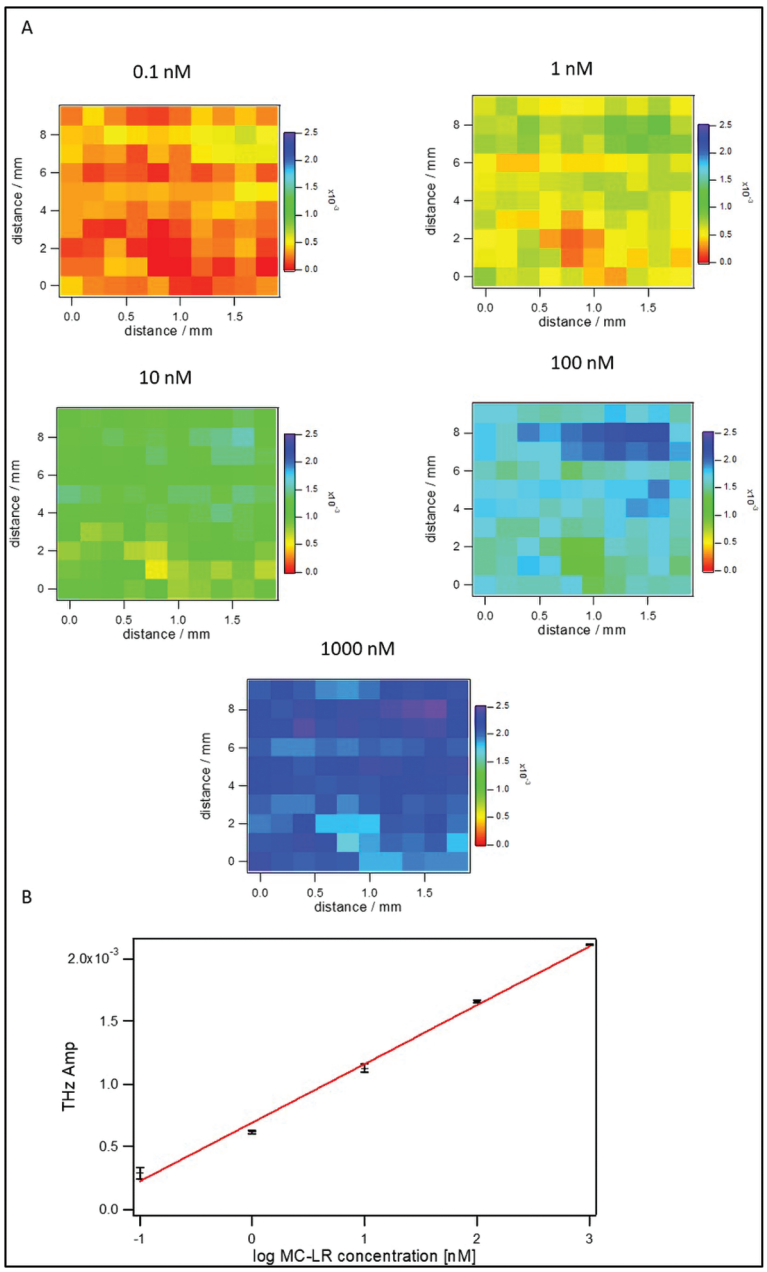

Fig. 5 MC-LR detection [A] THz peak amplitude mapping of the sensing plate at different concentrations of MC-LR. Each image is constructed by averaging three trials by using IGOR pro-2015. [B] THz amplitude (V) plotted *versus* log number of MC-LR concentration. Each THz amplitude was estimated by averaging its corresponding TCM image. All THz values are presented as means ± S.E.M of three trials. The equation $\sqrt{\Delta X^2 + \Delta Y^2}$ is used to calculate the S.E.M. for each THz value. Here, ΔX and ΔY are S.E.M. values for the baseline (buffer) and spiked samples with different MC-LR concentrations, respectively. This formula has been used because we subtracted two independent errors, and thus the two errors tend to cancel out each other, so they are accumulated in quadrature. The LOD was estimated by multiplying the S.E.M. of the lowest concentration by 3 (3× S.E.M) and then added to the zero background. The lowest THz signal that the TCM can detect is about 0.00008 V. Ultimately, the lowest concentration that can be measured by the TCM system, by using the linear function, would be around 0.05 nM (50 ng L^{-1}).

pH 7.4. We found that the change in the THz signal with MC-LR was much higher than that with kanamycin and ampicillin. However, the change in the THz signal of kanamycin cannot be ignored (Fig. S9†). This phenomenon might be explained by nonspecific interactions between kanamycin, positively charged and negatively charged sugar-phosphate backbone of DNA. To eliminate nonspecific interactions, we increased the concentration of the Mg^{2+} ions in the binding and washing buffer to 10 mM. Divalent ions such as Mg^{2+} cations can modulate these interactions by reducing the charge polarization of the phosphate groups in DNA toward positively charged amino groups in kanamycin molecules.[49] A

Table 1 Experimental results of the detection of MC-LR in a complex water sample spiked with 0.1 nM of MC-LR

Sample	MC-LR concentration (nM)	Change in THz signal (mV) ± S.E.M of 3 trials	Recovery (%)
Non-spiked buffer		0.438[a]±0.181	
Non-spiked complex		0.248[a]±0.130	
Non-spiked complex + 0.1 v of 10× buffer		0.480 ± 0.124	
Spiked buffer	0.1	0.335[b]±0.145	
Spiked complex	0.1	0.247[b]±0. 044	70
Spiked complex + 0.1 v of 10× buffer	0.1	0.327 ± 0.021	94

[a] THz amplitude of non-spiked samples − THz amplitude of the TCM sensor without samples. [b] THz amplitude of spiked samples − THz amplitude of non-spiked samples.

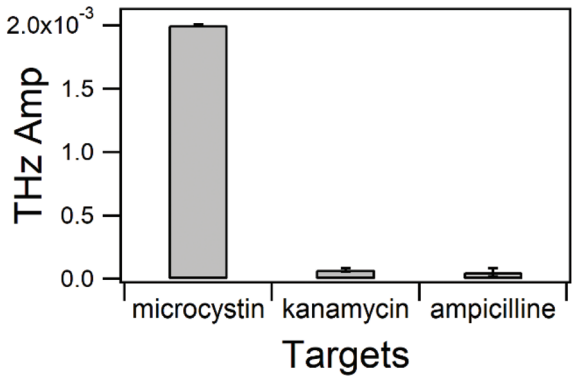

Fig. 6 TCM response to 1 μM of MC-LR, kanamycin, and ampicillin. These targets are prepared in the binding buffer that contains 10 mM of Mg^{2+} ion concentration. All THz values are presented as means ± S.E.M of three trials. The equation $\sqrt{\Delta X^2 + \Delta Y^2}$ is used to estimate the S.E.M. for each THz value. Here, ΔX and ΔY are S.E.M. values for the baseline (buffer) and spiked samples with microcystin, kanamycin, and ampicillin.

shown in Fig. 6, this procedure allows the TCM aptasensor to have a high selectivity toward MC-LR.

Conclusion

We succeeded in developing and optimizing a new aptasensor based on THz emission technology for highly sensitive detection of small molecules such as MC-LR in a complex "real-world" water sample, especially when adjusted with buffer. The LOD and the detection time of the TCM aptasensor are around 50 ng L^{-1} and 15 min, respectively, which provides a highly sensitive and rapid biosensor compared with other methods such as SPR and ELISA. In addition, the TCM sensor is highly specific to MC-LR with selectivity against other targets. Finally, we demonstrate that the sensitivity of the TCM sensor has been improved by efficiently optimizing the adsorption of the aptamer on the surface as well as the binding of MC-LR with aptamers.

Conflicts of interest

There are no conflicts to declare.

Acknowledgements

We acknowledge the support of the Natural Sciences and Engineering Research Council of Canada (NSERC). We also wish to thank Compute Canada for the computing infrastructure required for active cell calculations.

References

1 R. Peltomaa, B. Glahn-Martinez, E. Benito-Pena and M. C. Moreno-Bondi, *Sensors*, 2018, **18**(12), 4126.
2 S. L. Znoyko, A. V. Orlov, A. V. Pushkarev, E. N. Mochalova, N. V. Guteneva, A. V. Lunin, M. P. Nikitin and P. I. Nikitin, *Anal. Chim. Acta*, 2018, **1034**, 161–167.
3 X. Wang, L. Cohen, J. Wang and D. R. Walt, *J. Am. Chem. Soc.*, 2018, **140**, 18132–18139.
4 G. Brandhorst, M. Oellerich, G. Maine, P. Taylor, G. Veen and P. Wallemacq, *Clin. Chem.*, 2012, **58**, 821–825.
5 X. L. Fu, L. X. Chen and J. Choo, *Anal. Chem.*, 2017, **89**, 124–137.
6 B. J. Yakes, S. Prezioso, S. A. Haughey, K. Campbell, C. T. Elliott and S. L. DeGrasse, *Sens. Actuators, B*, 2011, **156**, 805–811.
7 E. Dittmann and C. Wiegand, *Mol. Nutr. Food Res.*, 2006, **50**, 7–17.
8 W. W. Carmichael, *J. Appl. Bacteriol.*, 1992, **72**, 445–459.
9 I. Y. Massey, X. Zhang and F. Yang, *J. Toxicol. Environ. Health, Part B*, 2018, **21**, 357–369.
10 C. Mackintosh, K. A. Beattie, S. Klumpp, P. Cohen and G. A. Codd, *FEBS Lett.*, 1990, **264**, 187–192.
11 I. Y. Massey, F. Yang, Z. Ding, S. Yang, J. Guo, C. Tezi, M. Al-Osman, R. B. Kamegni and W. M. Zeng, *Toxicon*, 2018, **151**, 156–162.
12 O. World Health and S. International Programme on Chemical, Guidelines for drinking-water quality., *World Health Organization*, 1996, **2** https://apps.who.int/iris/handle/10665/38551.
13 L. A. Lawton, C. Edwards and G. A. Codd, *Analyst*, 1994, **119**, 1525–1530.
14 Q. Y. Li, L. L. Lian, X. Y. Wang, R. N. Wang, Y. Y. Tian, X. Y. Guo and D. W. Lou, *J. Sep. Sci.*, 2017, **40**, 1644–1650.
15 D. O. Mountfort, G. Kennedy, I. Garthwaite, M. Quilliam, P. Truman and D. J. Hannah, *Toxicon*, 1999, **37**, 909–922.
16 S. Nagata, H. Soutome, T. Tsutsumi, A. Hasegawa, M. Sekijima, M. Sugamata, K. Harada, M. Suganuma and Y. Ueno, *Nat. Toxins*, 1995, **3**, 78–86.
17 W. J. Fischer, I. Garthwaite, C. O. Miles, K. M. Ross, J. B. Aggen, A. R. Chamberlin, N. R. Towers and D. R. Dietrich, *Environ. Sci. Technol.*, 2001, **35**, 4849–4856.

18 A. Ng, R. Chinnappan, S. Eissa, H. C. Liu, C. Tlili and M. Zourob, *Environ. Sci. Technol.*, 2012, **46**, 10697–10703.
19 W. Vornholt, M. Hartmann and M. Keusgen, *Biosens. Bioelectron.*, 2007, **22**, 2983–2988.
20 M. Tonouchi, *Nat. Photonics*, 2007, **1**, 97–105.
21 M. Naftaly, N. Vieweg and A. Deninger, *Sensors*, 2019, **19**(19), 4203.
22 P. U. Jepsen, D. G. Cooke and M. Koch, *Laser Photonics Rev.*, 2011, **5**, 124–166.
23 H. Guerboukha, K. Nallappan and M. Skorobogatiy, *Adv. Opt. Photonics*, 2018, **10**, 843–938.
24 M. J. Tang, Q. Huang, D. S. Wei, G. Z. Zhao, T. Y. Chang, K. Kou, M. Wang, C. L. Du, W. L. Fu and H. L. Cui, *J. Biomed. Opt.*, 2015, **20**(9), 095009.
25 T. Kiwa, S. Oka, J. Kondo, I. Kawayama, H. Yamada, M. Tonouchi and K. Tsukada, *Jpn. J. Appl. Phys., Part 2*, 2007, **46**, L1052–L1054.
26 E. M. Hassan, A. Mohamed, M. C. DeRosa, W. G. Willmore, Y. Hanaoka, T. Kiwa and T. Ozaki, *Sens. Actuators, B*, 2019, **287**, 595–601.
27 C. L. Hu, N. Q. Gan, Y. Y. Chen, L. J. Bi, X. E. Zhang and L. R. Song, *Talanta*, 2009, **80**, 407–410.
28 X. C. Zhang and D. H. Auston, *J. Appl. Phys.*, 1992, **71**, 326–338.
29 X. C. Zhang, B. B. Hu, J. T. Darrow and D. H. Auston, *Appl. Phys. Lett.*, 1990, **56**, 1011–1013.
30 Z. Zhang and J. T. Yates, *Chem. Rev.*, 2012, **112**, 5520–5551.
31 G. Kresse and J. Hafner, *Phys. Rev. B: Condens. Matter Mater. Phys.*, 1993, **47**, 558–561.
32 G. Kresse and J. Hafner, *Phys. Rev. B: Condens. Matter Mater. Phys.*, 1994, **49**, 14251–14269.
33 G. Kresse and J. Furthmuller, *Comput. Mater. Sci.*, 1996, **6**, 15–50.
34 G. Kresse and J. Furthmuller, *Phys. Rev. B: Condens. Matter Mater. Phys.*, 1996, **54**, 11169–11186.
35 J. P. Perdew, K. Burke and M. Ernzerhof, *Phys. Rev. Lett.*, 1996, **77**, 3865–3868.
36 V. P. Glibin, M. Cherif, F. Vidal, J. P. Dodelet, G. X. Zhang and S. H. Sun, *J. Electrochem. Soc.*, 2019, **166**, F3277–F3286.
37 C. E. Szakacs, M. Lefevre, U. I. Kramm, J. P. Dodelet and F. Vidal, *Phys. Chem. Chem. Phys.*, 2014, **16**, 13654–13661.
38 Q. L. Wei, M. Cherif, G. X. Zhang, A. Almesrati, J. T. Chen, M. J. Wu, N. Komba, Y. F. Hu, T. Regier, T. K. Sham, F. Vidal and S. H. Sun, *Nano Energy*, 2019, **62**, 700–708.
39 T. Asset and P. Atanassov, *Joule*, 2020, **4**, 33–44.
40 J.-P. Dodelet, *Electrocatalysis in Fuel Cells: A Non- And Low-Platinum Approach*, 2013.
41 M. McKeague, *Int. J. Mol. Sci.*, 2017, **18**(10), 2212.
42 J. Q. Li, S. S. Wijeratne, X. Y. Qiu and C. H. Kiang, *Nanomaterials*, 2015, **5**, 246–267.
43 M. G. Antoniou, A. A. de la Cruz and D. D. Dionysiou, *J. Environ. Eng.*, 2005, **131**, 1239–1243.
44 A. Lavin, J. de Vicente, M. Holgado, M. F. Laguna, R. Casquel, B. Santamaria, M. V. Maigler, A. L. Hernandez and Y. Ramirez, *Sensors*, 2018, **18**(7), 2038.
45 F. Long, M. He, A. N. Zhu and H. C. Shi, *Biosens. Bioelectron.*, 2009, **24**, 2346–2351.
46 W. Ma, W. Chen, R. R. Qiao, C. Y. Liu, C. H. Yang, Z. K. Li, D. H. Xu, C. F. Peng, Z. Y. Jin, C. L. Xu, S. F. Zhu and L. B. Wang, *Biosens. Bioelectron.*, 2009, **25**, 240–243.
47 Y. Wang, A. Partridge and Y. Wu, *Talanta*, 2019, **198**, 350–357.
48 J. Homola, S. S. Yee and G. Gauglitz, *Sens. Actuators, B*, 1999, **54**, 3–15.
49 A. A. Farcaş and A. Bende, *Molecules*, 2019, **24**(23), 4249.